Thermal State, Slab Metamorphism, and Interface Seismicity in the Cascadia Subduction Zone Based On 3-D Modeling

Ji, Yingfeng
Yoshioka, Shoichi
Banay ,Yuval A.

(Citation)
Geophysical research letters,44(18):9242-9252

(Issue Date)
2017-09-28

(Resource Type)
journal article

(Version)
Version of Record

(URL)
https://hdl.handle.net/20.500.14094/90005023

AGU PUBLICATIONS

Geophysical Research Letters

RESEARCH LETTER
10.1002/2017GL074826

Key Points:
- Oblique subduction results in asymmetric thermal and dehydration regime especially beneath north Cascadia
- Three-dimensional intraslab dehydration distribution is highly concerned with the 3-D distribution of the slow and regular earthquakes in Cascadia
- Tectonic tremors occurring at Cascadia are very probably attributed to the slab amphibolization eclogitization and fluid overpressurization

Supporting Information:
- Supporting Information S1

Correspondence to:
Y. Ji,
jiyf@people.kobe-u.ac.jp

Citation:
Ji, Y., Yoshioka, S., & Banay, Y. A. (2017). Thermal state, slab metamorphism, and interface seismicity in the Cascadia subduction zone based on 3-D modeling. *Geophysical Research Letters*, *44*, 9242–9252. https://doi.org/10.1002/2017GL074826

Received 7 JUN 2017
Accepted 29 AUG 2017
Accepted article online 5 SEP 2017
Published online 18 SEP 2017

Thermal State, Slab Metamorphism, and Interface Seismicity in the Cascadia Subduction Zone Based On 3-D Modeling

Yingfeng Ji[1], Shoichi Yoshioka[1,2], and Yuval A. Banay[2]

[1]Research Center for Urban Safety and Security, Kobe University, Kobe, Japan, [2]Department of Planetology, Graduate School of Science, Kobe University, Kobe, Japan

Abstract Giant earthquakes have repeatedly ruptured the Cascadia subduction zone, and similar earthquakes will likely also occur there in the near future. We employ a 3-D time-dependent thermomechanical model that incorporates an up-to-date description of the slab geometry to study the Cascadia subduction thrust. Results show a distinct band of 3-D slab dehydration that extends from Vancouver Island to the Seattle Basin and farther southward to the Klamath Mountains in northern California, where episodic tremors cluster. This distribution appears to include a region of increased dehydration in northern Cascadia. The phenomenon of heterogeneous megathrust seismicity associated with oblique subduction suggests that the presence of fluid-rich interfaces generated by slab dehydration favors megathrust seismogenesis in the northern part of this zone. The thin, relatively weakly metamorphosed Explorer, Juan de Fuca, and Gorda Plates are associated with an anomalous lack of thrust earthquakes, and metamorphism that occurs at temperatures of 500–700°C near the Moho discontinuity may represent a key factor in explaining the presence of the associated episodic tremor and slip (ETS), which requires a young oceanic plate to subduct at a small dip angle, as is the case in Cascadia and southwestern Japan. The 3-D intraslab dehydration distribution suggests that the metamorphosed plate environment is more complex than had previously been believed, despite the existence of channeling vein networks. Slab amphibolization and eclogitization near the continental Moho depth is thus inferred to account for the resultant overpressurization at the interface, facilitating the generation of ETS and the occurrence of small to medium thrust earthquakes beneath Cascadia.

1. Introduction

Historically, great earthquakes have repeatedly shaken Cascadia and have devastated the fragile regions along the coasts of Vancouver Island, Oregon, and Washington, as is known from plant-based evidence of coseismic subsidence (e.g., Atwater et al., 1991; Atwater & Yamaguchi, 1991; Nelson, 1992; Yamaguchi et al., 1997; Nelson et al., 2006), cultural records (e.g., Satake et al., 1996; Tsuji et al., 1998), and analysis of marine turbidites (Goldfinger et al., 2012). The most recent *M* 9 class earthquake occurred in 1700, and the earthquake recurrence interval seems to have been approximately 500 years along the Cascadian coastal margin during the Holocene (e.g., Goldfinger et al., 2012). However, the details of the mechanism responsible for these tsunamigenic great earthquakes are still unclear, and no mega earthquakes have been detected instrumentally along this coastal zone. In contrast to the constant and typically clustered megathrust earthquakes that occur on the cold and thick Pacific (PAC) Plate as it subducts beneath northeastern Japan (a handful of tremors and interface slips have also occurred there), the warm and young Juan de Fuca (JF) Plate that is subducting beneath the North American (NA) Plate witnesses the occurrence of far fewer earthquakes but abundant episodic tremor and slip (ETS) in Cascadia. A comparison of these two differing seismic zones is intriguing and may provide additional insight into the tectonic setting and environment required for the occurrence of ETS in Cascadia.

The repeated slow slip events observed in northern Cascadia are accompanied by unique tremor-like seismic signatures with an average interval of 13 to 16 months identified from crustal motion data spanning 6 years (e.g., Miller et al., 2002; Rogers & Dragert, 2003; Schmidt & Gao, 2010). ETS activity is a real-time indicator of stress loading of the Cascadia megathrust earthquake zone (Rogers & Dragert, 2003). Strictly speaking, the definition of a seismogenic zone depends on the size of the earthquakes used to define it (Wang & Tréhu, 2016). Because much of the locked zone in Cascadia is offshore, and most of the geodetic observations to

date have been made on land, most currently used geodetically inferred seismogenic zones are severely model dependent. The *M* 9.0 Tohoku-oki earthquake has shown that the small and medium earthquakes span a wide range of depths from shallower than 30 km to deeper than 60 km along the creeping segment of the fault (Wang & Tréhu, 2016). Many $>M$ 2.0 intraslab earthquakes have occurred beneath Tohoku on highly dehydrated fault segments along the Pacific Plate, and their distribution is found to coincide with the 3-D spatial variation of the slab dehydration regime (Ji et al., 2016, 2017).

The definition of the seismic zone that is based on small to medium earthquakes (Wang & Tréhu, 2016) is used in this study because the Gutenberg-Richter law states that the occurrence of seismicity follows an exponential distribution within individual regions. According to this law, great earthquakes are likely to be embedded in observable small earthquakes. This statement is particularly useful in studying subduction zones such as Cascadia that lack sufficient instrumentally recorded mega earthquakes but where inland small seismic events are usually detected.

Compared with the seismicity inland Cascadia, detected interplate seismicity at offshore central Cascadia from the hypocenter catalog determined by seismic network and limited offshore ocean bottom seismometer (OBS) data is anomalously deficient (Wang & Tréhu, 2016). The only exception to the deficiency may be the hypothesized interaction between a subducted seamount offshore of central Oregon (Tréhu et al., 2012) and several events offshore Vancouver Island. The low background seismicity offshore makes Cascadia atypical among the various circum-Pacific margins; however, beneath western Washington, Wadati-Benioff zone epicenters and fore-arc epicenters overlap between slab depth of 40–50 km (McCrory et al., 2012), as shown in Figure 1, the seismicity from 2001 to 2010 and detected tectonic tremors on the thrust fault beneath western Washington and the Seattle Basin. Profuse seismicity also occurs south of Cape Blanco near the junction between the PAC, NA, and Gorda Plates and the area offshore of Vancouver Island near the junction between the JF, NA, and Explorer Plates. The triple junction dynamics and upper plate tectonics may have impact on these earthquakes; however, interplate earthquakes are rarely detected within the inland parts of Cascadia, such as western British Columbia, Oregon, and northeastern California, contrasting with those zones with frequently detected seismicity at Vancouver Island and Washington.

One of candidates to explain these differences in seismicity frequency is the occurrence of slab brittle failure, which is controlled by the thermal states of the slabs, pore fluid pressures, and the reductions in shear strength that result from slab metamorphism that could potentially change the fault strength. Numerous previous studies have contrasted warm and cool subduction zones (e.g., Peacock & Wang, 1999). Wada and Wang (2009) used Cascadia and Japan Trench as end-member warm and cold subduction zones and discussed the stability conditions of hydrous minerals but did not calculate the amounts of fluid released by the slab and consumed by the mantle wedge. Gao and Wang (2017) followed the same logic and applied the concepts to ETS. Abers et al. (2013) contrast the location of earthquakes in young and cold plates, including northern Japan and Cascadia, and link these differences to dehydration reactions. Abers et al. (2017) make a similar point that only warm-slab subduction zones see highly hydrated mantle wedge corner. The effect of the geometry of the JF Plate on the Wadati-Benioff zone seismicity has been discussed (McCrory et al., 2012), but this phenomenon has not yet been integrated into 3-D thermal modeling. The plate convergence direction in Cascadia ranges from approximately N35°E in the southernmost part of the Cascadia Trench to N50°E in the northernmost part (DeMets et al., 2010). On the other hand, the trench-normal azimuth is N75°E, which represents a subduction obliquity of nearly 30° (Figure 1). This level of obliquity affects the heterogeneous slab temperature structure in subduction zones like that of southwestern Japan (Ji & Yoshioka, 2017). In this regard, it is necessary to reevaluate the heterogeneity or irregularity of the thermal regime and slab dehydration, both at the plate boundaries and inside the subducted oceanic plate in Cascadia, as represented by 3-D numerical simulations. This effort may shed light on the process of slab metamorphism in this young, hot plate subducting beneath the Pacific Northwest.

2. Methods and Models

To explore the three-dimensional slab thermal state and the process of petrological metamorphism at Cascadia, we constructed a 3-D, time-evolving thermomechanical model based on stag3d (Tackley & Xie, 2003) that has dimensions of 1150 × 700 × 400 km (length × width × depth) and simulates the

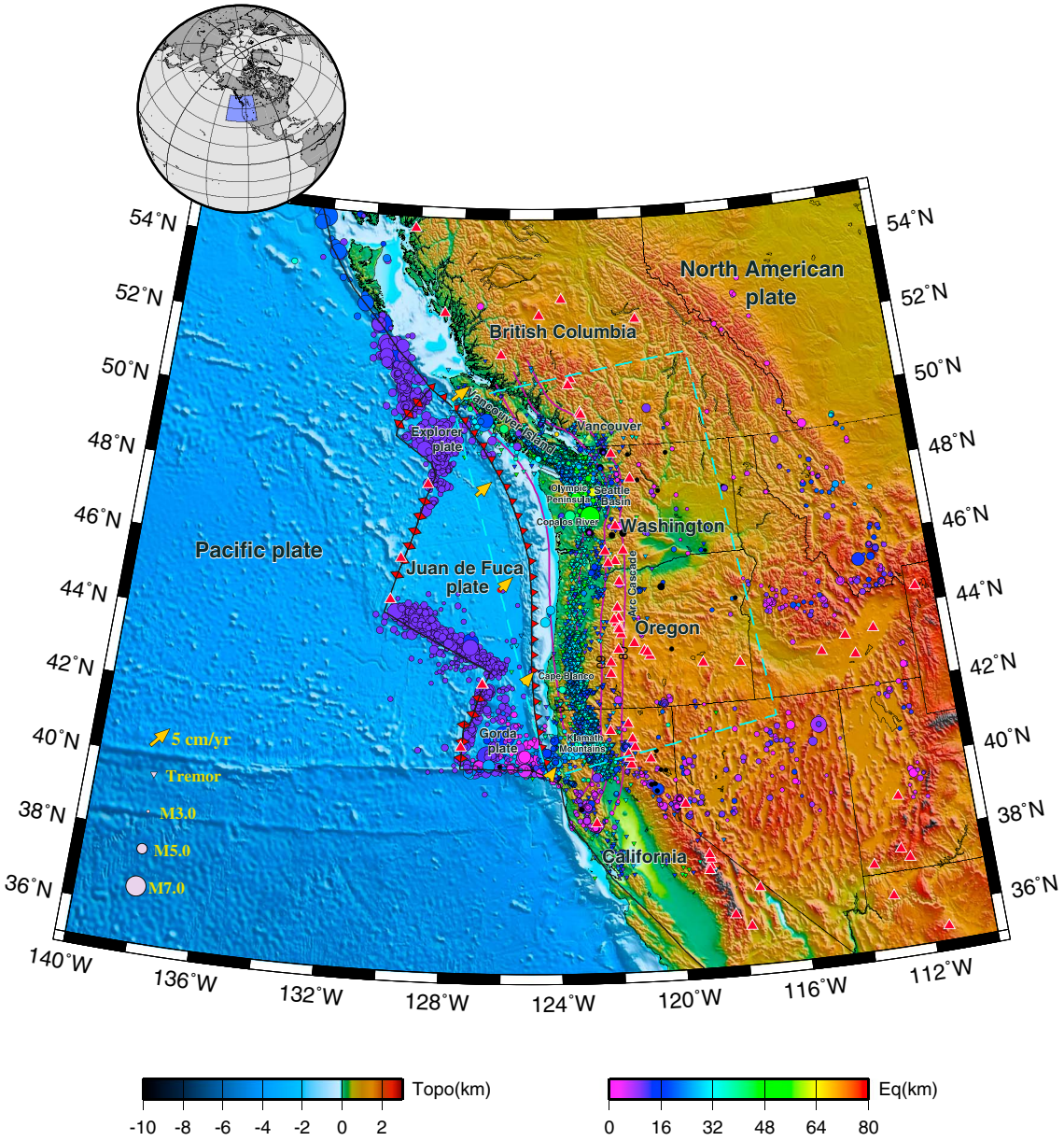

Figure 1. Tectonic map of Cascadia. Background colors indicate the surface topography (ETOPO) (Smith & Sandwell, 1997). Violet curved lines indicate the isodepth contours of the upper surfaces of the Explorer, JF, and Gorda Plates with an interval of 20 km (Slab 1.0) (Hayes et al., 2012). Dashed light blue lines show the model region for the subducted Explorer, JF, and Gorda Plates. Small inverted triangles show the distribution of the epicenters of tectonic tremors during the period extending from 9 January 2005 to 31 December 2012 with magnitude less than 3.0, following the world tremor database (Ide, 2010, 2012; Idehara et al., 2014). The depths of hypocenters are indicated with colors. Yellow arrows illustrate the motion of the Explorer, JF, and Gorda Plates with respect to the NA Plate. Red triangles indicate active volcanoes (Siebert et al., 2010). Red barbed lines mark the convergent or divergent plate boundaries.

simultaneous penetration of the Explorer, JF, and Gorda Plates northeastward over 15 Myr. The geometry of the Explorer, JF, and Gorda Plates is well constrained by Slab 1.0 (Hayes et al., 2012), and it is extrapolated within the modeled domain. The oceanic lithospheric thickness is prescribed to be initially 16 km at the trench and reaches 30 km, according to the spatial distribution of crustal age. The trenchward temperature boundary follows a plate cooling model (Grose & Afonso, 2013), and the plate ages are provided by EarthByte (Muller et al., 2008). Compared with Tohoku in Japan, the oceanic lithosphere in Cascadia is very young and hot; seafloor ages of 6–8 Myr occur at the trench approaching Oregon and Vancouver Island, whereas ages of 4–6 Myr occur along its central segment offshore from Washington (Figure S1 in the

supporting information). The plate ages are used to simulate the thermal state of the incoming plate. Observations of surface heat flow average 30–50 mW/m^2 (Pollack et al., 1993) west of the Cascade Range in Cascadia, where the thrust depth is 20–60 km, revealing an existence of cold fore-arc mantle wedge. The calculation is fit by observation along eight quasi-trench-perpendicular profiles passing through densely observed areas in Cascadia, excluding the expanding oceanic ridge where abnormally high surface heat flow exists (Figure S2). The heat flux offshore Cascadia averages 50–80 mW/m^2, and these values are higher than those observed offshore from Tohoku, Japan (20–50 mW/m^2, on average), due to the significantly hotter oceanic plate in Cascadia.

The subduction velocity is prescribed for the incoming plate following MORVEL (DeMets et al., 2010) in the Cascadia model. The plate motion reference is adopted at the center of Cascadia block which is in conformity with the NA plate motion. The vertical model boundaries and bottom are assumed to be adiabatic and permeable, while the top boundary is prescribed to be a fixed temperature (0°C) and rigid. The viscosity for wet olivine was obtained from Hirth and Kohlstedt (2003) and Burkett and Billen (2010). The observations of surface heat flow used to constrain the model thermal regime are available from the global heat flow database (Pollack et al., 1993) (see Figure S2). Other model configuration options and parameters are described in the supporting information.

Beneath the thick sediment, mid-ocean ridge basalts (MORBs) are believed to be the major constituent of the uppermost parts of oceanic plates (Omori et al., 2009), and peridotite and gabbro make up the ultramafic rocks underneath (Hacker et al., 2003). We inferred the 3-D distribution of the slab hydration state in these two layers inside the downgoing oceanic plate based on the calculated 3-D thermal results and slab depth. Therefore, the spatial variations of the slab dehydration and mineralogical phase transitions can be more accurately estimated in 2-D thermomechanical models at depth (Ji & Yoshioka, 2015; Gao et al., 2017) in places where curved plates undergo obvious oblique subduction.

3. Results and Discussion

3.1. Three-Dimensional Temperature Structure and Temperature Gradient

The calculated thermal regime of the subducted Explorer, JF, and Gorda Plates in Cascadia presents a thrust zone with interplate temperature spanning from 300°C to 500°C between the Cascadia trench and the onshore area, favoring thermally controlled brittle failure (Figure 2a). The result is generally consistent with the thermally controlled seismogenic and transition zones determined from geodetic constraints or the inversion of elastic dislocation models using horizontally and vertically distributed data (McCaffrey et al., 2013; Hyndman, 2013; Wang & Tréhu, 2016), and the inferred thermally controlled seismogenic zone covers the origins of the earthquakes that are occasionally observed offshore of Oregon. Cozzens and Spinelli (2012) produce a model that indicates the temperature on the subduction thrust at 300°C in agreement with this study. The featured local seismic activity is explainable because of the seismogenic behavior of gabbro in rate-and-state friction models at temperatures of 510°C in Cascadia (Liu & Rice, 2009). The hypocenters of ordinary interplate $>M$ 3.0 earthquakes that occurred from 1 January 2001 to 31 December 2010, as determined by Incorporated Research Institutions for Seismology (IRIS), are displayed by colored spheres that indicate the events (Figure 2). Both of the colors and the size of the spheres indicate the magnitude of the events. These events are particularly strongly clustered beneath Vancouver Island, the Seattle Basin, and the junction between the PAC, NA, and Gorda Plates, and some are sparsely distributed within the Olympic Peninsula and offshore of Oregon (Figures 1 and 2a). The sources of tectonic tremors (Ide, 2010, 2012; Idehara et al., 2014) are approximately distributed along the 700°C isotherm southward to the Klamath Mountains in northern California, except in the southeastern part of Vancouver Island (500°C–600°C); however, the local ETS is otherwise suggested to involve the entire southern portion of Vancouver Island (Boyarko et al., 2015). If so, the interplate temperature at the source region of the ETS beneath Vancouver Island could reach 700°C. The high interface temperatures associated with ETS activity are not commonly found in shallower megathrusts at subduction zones, which is possibly attributable to the presence of the fore-arc mantle corner in the vicinity of this depth (McCrory et al., 2014). In southwestern Japan, the temperature at the source region of tectonic tremors is estimated to be 400–700°C (Ji et al., 2016, 2017); in Cascadia, a majority of the ETS occurring at the plate boundary is thought to be associated with a temperature of 500–750°C (Figure 2) that is likely attributable to the downdip of the transition zone

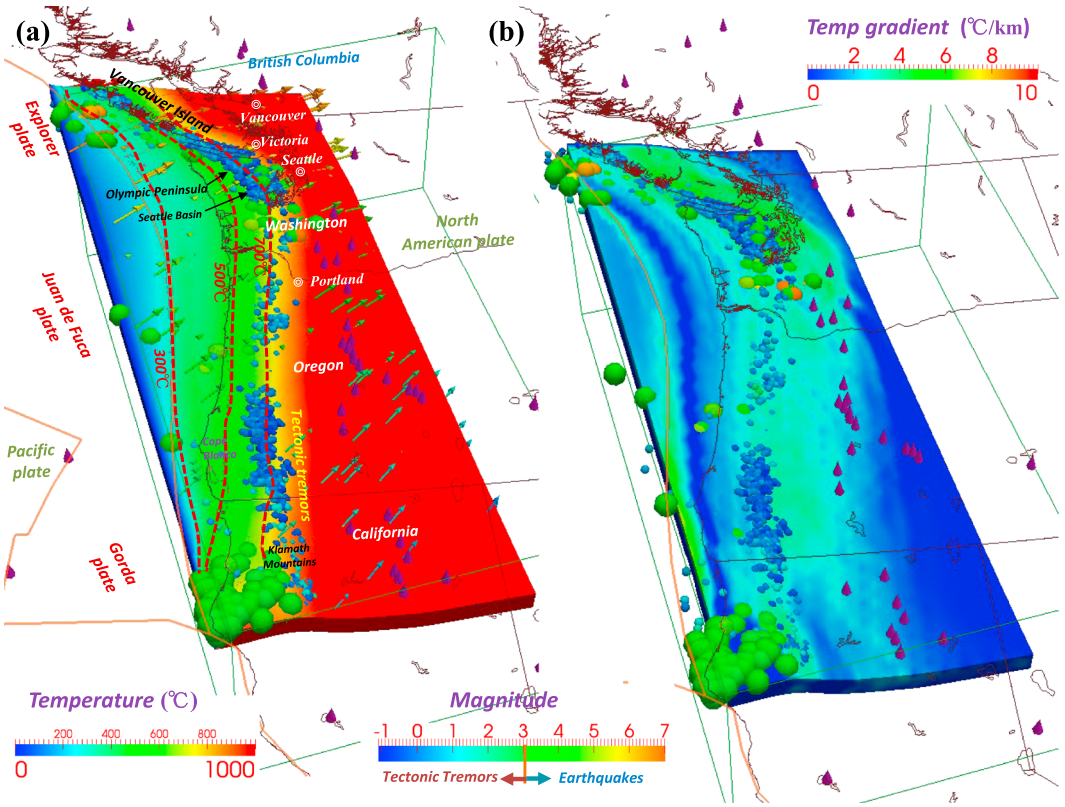

Figure 2. (a) The calculated temperature distribution on the upper surface of the Explorer, JF, and Gorda Plates. Colored spheres indicate regular interplate earthquakes with magnitudes greater than 3.0 (IRIS) that occurred during the period extending from 1 January 2001 to 31 December 2009. The plotted hypocenters are between 2 km above and 7 km below the interface. Small blue spheres indicate the epicenters of deep tectonic tremors with magnitudes less than 3.0 (Ide, 2010, 2012; Idehara et al., 2014) that occurred during the period extending from 9 January 2005 to 31 December 2012. Purple cones indicate active volcanoes (Siebert et al., 2010). (b) The calculated temperature gradient distribution on the upper surfaces of the Explorer, JF, and Gorda Plates.

from brittle deformation to ductile creep. Beneath Vancouver Island, the tremor occurs where a much higher temperature of 575 ± 50°C is predicted (Peacock, 2009) where ETS occurs at the shallowest depths in Cascadia, and this result agrees with this study. Predicted tremor temperatures less than 500°C by previous researches are possibly related to the effect of plate decoupling caused by hydrous plate interface with a low viscosity or a different temperature setting in the landward NA plate in previous models. If the plate decoupling is not involved, the interface temperature at Moho depth would probably reach 500–600°C. In addition, laboratory experiments have documented that the stick-slip behavior in pyroxene gouge can reach 550°C (He et al., 2013), indicating that the thermal range for seismic events is broader than was previously believed. Considering that the seismogenic Tohoku subduction megathrust is thought to have interplate temperatures of 200°C–600°C, the upper surface of the Explorer, JF, and Gorda Plates is hotter than that of the PAC Plate beneath Tohoku by 200–300°C on average. Moreover, the temperature of the upper surface of the subducting plate depends on the subduction of the slab with various subduction interface geometries; thus, the detailed 3-D properties of this subduction zone must be analyzed. We present Figure S7 to show the slab thermal state at a relative depth of 8 km, 16 km, and 24 km inside the incoming plate.

For the interplate thermal gradient along the subduction direction, since in southwest Japan the calculation of 3-D thermal model has shown abnormally high values near the source region of tectonic tremors in western Shikoku (Ji et al., 2016, 2017), we thus investigate the 3-D interplate thermal gradient distribution at Cascadia through the 3-D thermal modeling.

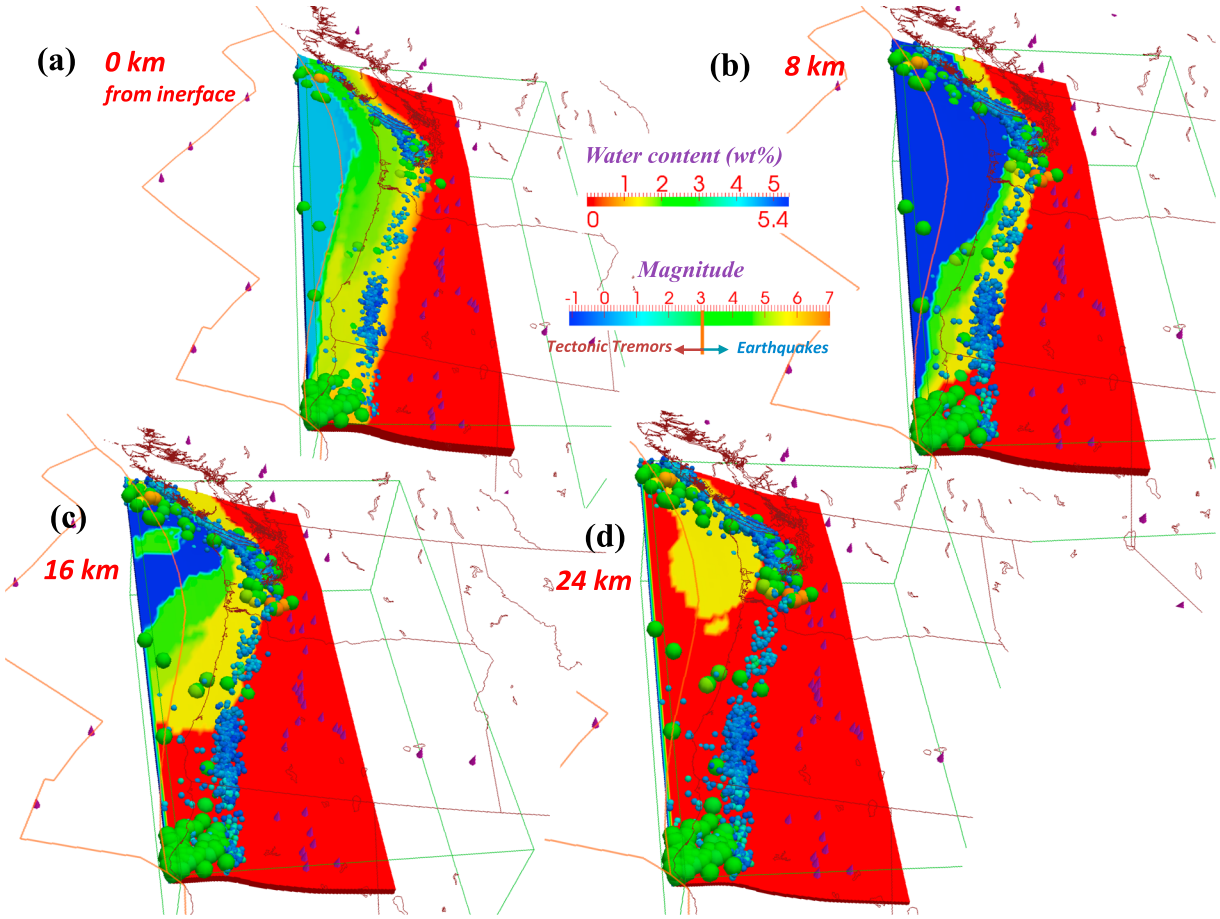

Figure 3. The calculated distributions of slab water content (wt %) on the four surfaces located at (a) 0 km, (b) 8 km, (c) 16 km, and (d) 24 km from the megathrust are shown. Colored spheres indicate regular interplate earthquakes with magnitudes greater than 3.0 (IRIS) that occurred during the period extending from 1 January 2001 to 31 December 2010. The plotted hypocenters are located between 2 km above and 7 km below the megathrust. Small blue spheres indicate the epicenters of deep tectonic tremors with magnitudes less than 3.0 (Ide, 2010, 2012; Idehara et al., 2014) that occurred during the period extending from 9 January 2005 to 31 December 2012.

Figure 2b shows the interplate temperature gradient on the upper surfaces of the Explorer, JF, and Gorda Plates. The thrust surface beneath Vancouver Island and the Seattle Basin has the highest temperature gradient (>5°C/km) within a depth range of 40–80 km, whereas the gradient associated with the corresponding plate boundary in Oregon decreases to <5°C/km; however, the gradient increases again in southern Oregon to nearly 4°C/km. This distribution reflects an asymmetric thermal state (Figure S7) on the Cascadia plate boundary that likely results from the oblique northeastward subduction, which has an azimuthal difference of 30°. Oblique subduction results in the difference between the subduction angles along curve slab geometry in north Cascadia and those in south Cascadia. Obliquity accompanied by thermal heterogeneity is speculated to occur at other subduction zones where the plate convergence possesses an obvious trench-parallel component and is reminiscent of southwestern Japan, where similar obliquity leads to the inference of a thermal gradient along the downdip direction at the depth of the Mohorovičić discontinuity (Ji & Yoshioka, 2015; Ji et al., 2016, 2017).

3.2. Water Content and Slab Dehydration

Estimates of the hydration state of the descending Explorer, JF, and Gorda Plates obtained using the 3-D thermomechanical model at various depths measured vertically downward from the thrust surface are displayed in Figure 3. The seismogenic zone located at the high water-content transition boundaries is identified beneath Vancouver Island and the Seattle Basin along the four interface-parallel surfaces (Figure 3), where regular earthquakes and clustered ETS events are well documented. The weaker activity of tremors in

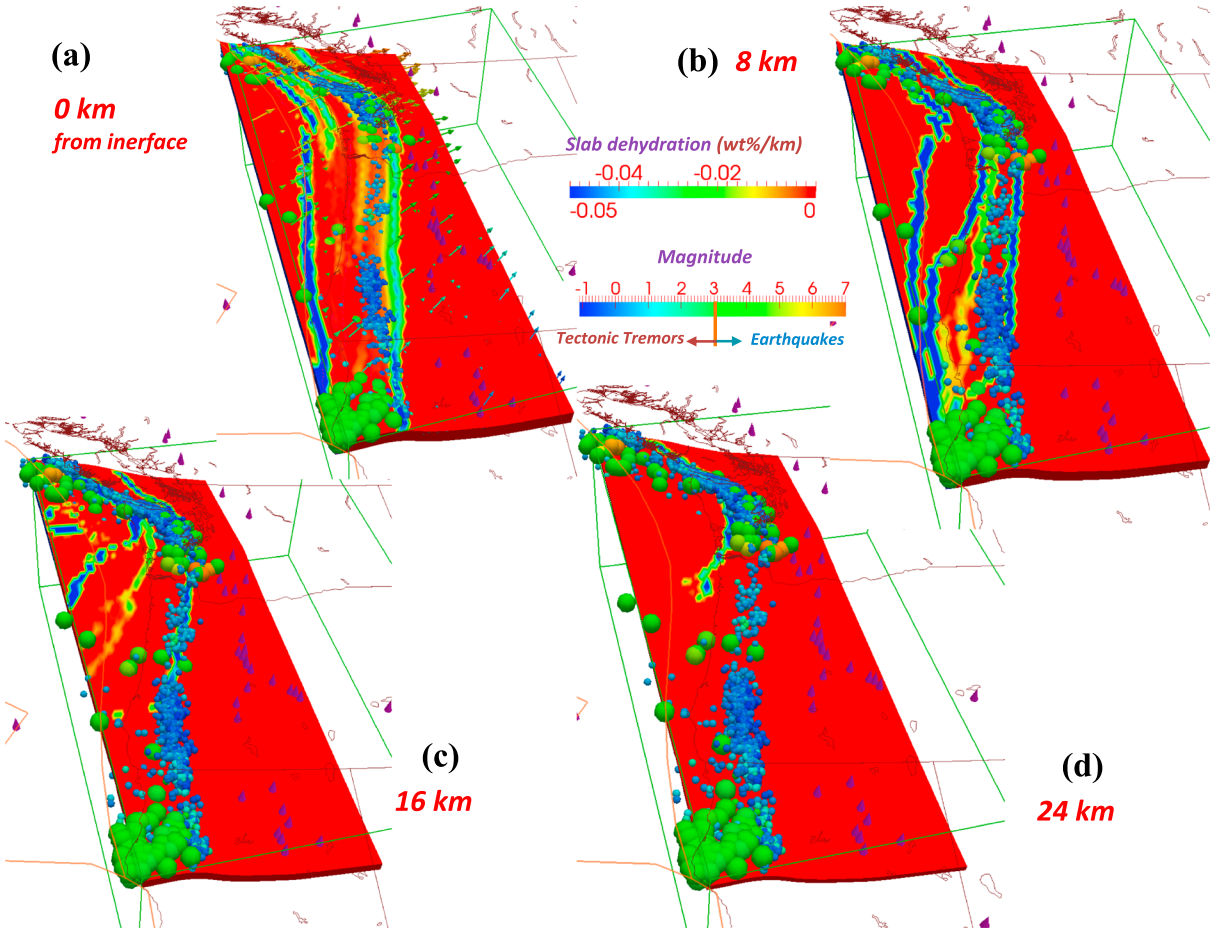

Figure 4. The calculated distributions of slab dehydration (wt %/km) on the four surfaces located at (a) 0 km, (b) 8 km, (c) 16 km, and (d) 24 km from the megathrust are shown. Symbols are the same as those used in Figure 3.

southern Oregon and northern California are favored by the existence of water-content transitions at depths of 0 and 8 km below the megathrust (Figures 3a and 3b). Since water-content transitions must be compared with the subduction direction, which helps determine the amount of dehydration, we calculate the rate of slab dehydration in a unit of wt %/km in this study (Figure 4).

The dehydration rate of the Explorer, JF, and Gorda Plates is distinctly elevated in northern Cascadia, especially along the interplate seismogenic zone that connects Vancouver Island, the Olympic Peninsula, and the Seattle Basin. The seismicity in western Oregon corresponds to the shallower intraslab portion, where MORB dehydration plays a more important role. The more continuous ETS episodes that occur in northern Cascadia and the larger number of tremors that initiate and migrate from there demonstrate that this environment is conducive to the occurrence of tectonic tremors and slow slip events. In addition, the significant expulsion of fluids due to slab dehydration in northern Cascadia coincides with evidence of seismic attenuation in northern Cascadia, especially Washington (a cold serpentinized mantle wedge is thought to exist beneath northwestern Washington and southwestern British Columbia (Brocher et al., 2003)), high pore pressures at a depth of 35 km beneath the southern part of Vancouver Island (Peacock et al., 2011) and Mount St Helens, which is adjacent to the Seattle Basin (Hansen et al., 2016). Bostock et al. (2002) also demonstrated the existence of a hydrated fore-arc mantle wedge under central Oregon (44.5°N). The hydrated mantle wedge accounts for the observed low surface heat flow, which was verified in this study by comparison with the model output. From the model results, we found that the maximum slab dehydration exceeds −0.05 wt %/km for the MORB layer and −0.1 wt %/km for the ultramafic layer. These results are similar to the amounts inferred for the plate interface in eastern Kyushu and the Bungo Channel in southwestern

Japan (which range up to −0.06 wt %/km). The segmentation of tremor episodes between northern, central, and southern Cascadia (Wang et al., 2013) could be a corollary of the along-strike perturbation in dehydration levels between northern and southern Cascadia (Figures 3 and 4), but additional evidence is needed to support this scenario.

Because the Explorer, JF, and Gorda Plates are particularly hot and thin, the corresponding fewer detected small-medium seismic events may imply that dehydration embrittlement caused by hot slab dehydration could be a candidate to interpret the genesis of small-medium earthquakes in Cascadia. In particular, if we do not regard great earthquakes occurring on locked faults as the only type of seismogenic zone for the purposes of disaster mitigation, the process of mineralogical metamorphism affecting the majority of small-medium earthquakes may be regarded as another type of seismogenic mechanism. Intraslab vertical fluid migration may be allowable, since the tremors in Cascadia display a reverse faulting mechanism that is commonly believed to reflect interface events where strong dilatancy occurs (Liu, 2013). In comparison, the intraslab tremors are less frequently detected; thus, the intraslab dilatancy is inferred to be weak, and there may be many fractures that channel the fluids produced by dehydration. The transport paths of fluids are also partly determined by the geometrical parameters of the fluid flow topology, such as vein networks, across a wide range of spatial scales (Plümper et al., 2017). This topology is likely affected by porosity, the distribution of dihedral angles, and the sizes and connectivity of fluid channels (Le Roux et al., 2013) and results in fluid flux or drainage in megathrusts (Nakajima & Hasegawa, 2016). In addition, the intraslab dehydration morphology itself seems to follow a complex 3-D distribution to a greater degree than is expected. Moreover, this distribution varies with depth, as seen from the differences among Figures 4a–4d. Of course, the fluid pathway is also not always strictly vertical and can follow the slab surface geometry or channels to form a complex pattern of slab-derived fluid transport or dissipation into the mantle or overriding plate (Wilson et al., 2014). A great earthquake may only result when triggered by small or slow earthquakes. Such earthquakes depend strongly on the plate boundary environment, and their detailed mechanisms are still debatable.

On the other hand, the ETS episodes that are typical of Cascadia have not been well replicated in other subduction zones, except southwestern Japan, where the recurrence intervals of geodetically detected slow slips are not as regular as those that occur in Cascadia (14 months) (Rogers & Dragert, 2003). We propose a possible explanation for the difference between the two subduction zones. The temperature background against which ETS occurs in Cascadia reaches nearly 700°C, which is consistent with the source region of nonvolcanic tectonic tremors that occur beneath the northern Bungo Channel and typically migrate to the east of Shikoku, indicating that a temperature threshold for creep deformation of 600–700°C, a Mohorovičić depth of 30–40 km, and a pressure of nearly 1 GPa could be the environment that favors episodic tremors and deep slow slips (shallow slow slips may be attributable to mechanical dehydration of the uppermost sediment layer) (e.g., Ellis et al., 2015). A young subducted oceanic lithosphere (<40 Myr) with a small dip angle above the Mohorovičić depth meets these two requirements, and this interpretation can explain why cold subduction zones lack these tremor episodes. Put simply, the slab thickness determines the dehydration budget and the earthquake activity, and the fluid content and temperature of the slab determine the activity level of tectonic tremors and deep slow slips.

3.3. Phase Transitions and Mineralogical Metamorphism

As discussed in section 3.2, insufficient slab dehydration in the ultramafic slab (Hacker et al., 2003) more than 7 km vertically downward from the interface lowers the activity of ordinary earthquakes in Cascadia. For hydrous MORB (Figures 3a and 4a), a band of increased dehydration and subsequently increased fluid flux occurs offshore, and this band corresponds to the prehnite-actinolite (PA; 4.4 wt %) phase transition or the conversion of greenschist (3.0 wt %) to amphibole (1.5–2.5 wt %) and finally eclogite (0 wt %), according to the relevant phase diagram of Omori et al. (2009) (Figure S8). Of these transitions, the change in mineral composition from greenschist (3.0 wt %) to eclogite (0 wt %) is the critical process that dominates the source region of ETS, which forms a band that extends from Vancouver Island to northern California. The transition in mineral assemblages from PA (4.4 wt %) to greenschist (3.0 wt %) may contribute to occurrence of thrust earthquakes offshore; however, the amount of fluid produced is <50% of that produced by MORB amphibolization and eclogitization. Meanwhile, in the ultramafic layer of the lower slab (Figures 3b–3d and 4b–4d), the dehydration of serpentinite chlorite brucite (15 wt %) or dunite (6.2 wt %) is absolutely prevalent in areas approaching northern Cascadia (Figures 3c and 4c), which features additional seismicity and tectonic

tremors. In Figure 3d, the yellow patch on the megathrust indicates chlorite harzburgite (1.4 wt %), which dewaters to garnet harzburgite (0 wt %) and still favors the northern Cascadia mantle wedge corner (Figure 4d). The presence of the oblique subduction megathrust, which favors dewatering of both MORBs and ultramafic rocks (Hacker et al., 2003), shows that the metamorphism of greenschist (3.0 wt %) to eclogite (0 wt %) occurs to a significant degree during the process of plate subduction and favors the Vancouver Island-Seattle Basin seismogenic band.

The P-T path for megathrust earthquakes, which resembles that seen in southwestern Japan, has a low slope and reaches the eclogite zone at a depth of 60 km (2 GPa). The metamorphic process that corresponds to 600–700°C and a depth of 40 km (1.33 GPa) is the amphibole-eclogite transition, which likely accounts for the generation of ETS. Moreover, the effects of fluid migration (Hyndman et al., 2015) from the most dehydrated portion of the slab (which occurs at depths of 50–60 km, immediately at the phase boundary) into the mantle wedge corner (which occurs at depths of 35–43 km) (McCrory et al., 2014) are included. Consequently, the similar P-T path in southwestern Japan suggests the existence of the amphibole-eclogite transition at nearly ~700°C at the fore-arc mantle wedge corner that is associated with ETS.

4. Conclusions

Through 3-D thermomechanical modeling of the Cascadia subduction megathrust and the downgoing oceanic lithosphere, we reached the following conclusions.

1. The relative lack of instrumentally recorded offshore earthquakes associated with the subduction of the hot and thin Explorer, JF, and Gorda Plates beneath Cascadia likely reflects a low level of slab dehydration compared with other cold subduction zones. An inferred plate interface temperature of ~700°C at the ETS source region, which is similar to the end-member of the northern Bungo Channel, southeastern Japan, suggests that the ETS likely is due to high temperatures.
2. Subduction obliquity contributes to the asymmetric thermal structure of the interface beneath the northern and southern parts of Cascadia, as well as the existence of asymmetric intraslab petrological dehydration near subduction interface.
3. A distinct band of slab dehydration extends from Vancouver Island through the Olympic Peninsula and the Seattle Basin to northern California. In particular, the northern half of Cascadia, which features megathrust seismicity and intermittent ETS episodes, includes a cold fore-arc mantle wedge, the existence of which is supported by evidence from seismic attenuation.
4. The metamorphism of greenschist (3.0 wt %) to eclogite (0 wt %) is dominant in the interplate ETS source. The low slope of the P-T path suggests that creep deformation during the amphibolization and eclogitization of MORB at the mantle wedge is associated with the generation of ETS.

Acknowledgments
We thank P. Tackley for sharing the original code of stag3d developed in this study. We thank IRIS for earthquake catalog and S. Ide for tectonic tremor catalog. We also thank I. Wada and two anonymous reviewers for their constructive comments allowed to improve this paper. This work was partly supported by Japan Society for the Promotion of Science grants KAKENHI 16H04040 and 16H06477. The data for this paper are available at DataOne database https://oneshare.cdlib.org/stash/dataset/doi:10.15146/R3909R.

References

Abers, G. A., Nakajima, J., van Keken, P. E., Kita, S., & Hacker, B. R. (2013). Thermal–petrological controls on the location of earthquakes within subducting plates. *Earth and Planetary Science Letters*, *369*, 178–187. https://doi.org/10.1016/j.epsl.2013.03.022

Abers, G. A., van Keken, P. E., & Hacker, B. R. (2017). The cold and relatively dry nature of mantle forearcs in subduction zones. *Nature Geoscience*, *10*, 333–337. https://doi.org/10.1038/ngeo2922

Atwater, B. F., & Yamaguchi, D. K. (1991). Sudden, probably coseismic submergence of Holocene trees and grass in coastal Washington State. *Geology*, *19*(7), 706–709. https://doi.org/10.1130/0091-7613(1991)019<0706:SPCSOH>2.3.CO;2

Atwater, B. F., Stuiver, M., & Yamaguchi, D. K. (1991). Radiocarbon test of earthquake magnitude at the Cascadia subduction zone. *Nature*, *353*(6340), 156–158. https://doi.org/10.1038/353156a0

Bostock, M., Hyndman, R., Rondenay, S., & Peacock, S. (2002). An inverted continental Moho and serpentinization of the forearc mantle. *Nature*, *417*, 536–538. https://doi.org/10.1038/417536a

Boyarko, D. C., Brudzinski, M. R., Porritt, R. W., Allen, R. M., & Tréhu, A. M. (2015). Automated detection and location of tectonic tremor along the entire Cascadia margin from 2005 to 2011. *Earth and Planetary Science Letters*, *430*, 160–170. https://doi.org/10.1016/j.epsl.2015.06.026

Brocher, T. M., Parsons, T., Tréhu, A. M., Snelson, C. M., & Fisher, M. A. (2003). Seismic evidence for widespread serpentinized forearc upper mantle along the Cascadia margin. *Geology*, *31*, 267–270. https://doi.org/10.1130/0091-7613(2003)031<0267:SEFWSF>2.0.CO;2

Burkett, E. R., & Billen, M. I. (2010). Three-dimensionality of slab detachment due to ridge-trench collision: Laterally simultaneous boudinage versus tear propagation. *Geochemistry, Geophysics, Geosystems*, *11*, Q11012. https://doi.org/10.1029/2010GC003286

Cozzens, B. D., & Spinelli, G. A. (2012). A wider seismogenic zone at Cascadia due to fluid circulation in subducting oceanic crust. *Geology*, *40*(10), 899–902. https://doi.org/10.1130/G33019.1

DeMets, C., Gordon, R. G., & Argus, D. F. (2010). Geologically current plate motions. *Geophysical Journal International*, *181*(1), 1–80. https://doi.org/10.1111/j.1365-246X.2009.04491.x

Ellis, S., Fagereng, A., Barker, D., Henrys, S., Saffer, D., Wallace, L., … Harris, R. (2015). Fluid budgets along the northern Hikurangi subduction margin, New Zealand: The effect of a subducting seamount on fluid pressure. *Geophysical Journal International*, *202*(1), 277–297. https://doi.org/10.1093/gji/ggv127

Gao, X., & Wang, K. (2017). Rheological separation of the megathrust seismogenic zone and episodic tremor and slip. *Nature*, *543*(7645), 416–419. https://doi.org/10.1038/nature21389

Gao, D., Wang, K., Davis, E. E., Jiang, Y., Insua, T. L., & He, J. (2017). Thermal state of the Explorer segment of the Cascadia subduction zone: Implications for seismic and tsunami hazards. *Geochemistry, Geophysics, Geosystems*, *18*(4), 1569–1579. https://doi.org/10.1002/2017GC006838

Goldfinger, C., Nelson, C. H., Morey, A. E., Johnson, J. R., Patton, J., Karabanov, E., … Vallier, T. (2012). Turbidite event history—Methods and implications for Holocene paleoseismicity of the Cascadia subduction zone. *U.S. Geological Survey Professional Paper*, 1661–F, 170.

Grose, C. J., & Afonso, J. C. (2013). Comprehensive plate models for the thermal evolution of oceanic lithosphere. *Geochemistry, Geophysics, Geosystems*, *14*, 3751–3778. https://doi.org/10.1002/ggge.20232

Hacker, B. R., Abers, G. A., & Peacock, S. M. (2003). Subduction factory: 1. Theoretical mineralogy, densities, seismic wave speeds, and H2O contents. *Journal of Geophysical Research*, *108*(B1), 2029. https://doi.org/10.1029/2001JB001127

Hansen, S. M., Schmandt, B., Levander, A., Kiser, E., Vidale, J. E., Abers, G. A., & Creager, K. C. (2016). Seismic evidence for a cold serpentinized mantle wedge beneath Mount St Helens. *Nature Communications*, *7*, 13242. https://doi.org/10.1038/ncomms13242

Hayes, G. P., Wald, D. J., & Johnson, R. L. (2012). Slab1.0: A three-dimensional model of global subduction zone geometries. *Journal of Geophysical Research*, *117*, B01302. https://doi.org/10.1029/2011JB008524

He, C., Luo, L., Hao, Q. M., & Zhou, Y. (2013). Velocity-weakening behavior of plagioclase and pyroxene gouges and stabilizing effect of small amounts of quartz under hydrothermal conditions. *Journal of Geophysical Research: Solid Earth*, *118*, 3408–3430. https://dx.doi.org/10.1002/jgrb.50280

Hirth, G., & Kohlstedt, D. (2003). Rheology of the upper mantle and the mantle wedge: A view from the experimentalists. In J. Eiler (Ed.), *Inside the Subduction Factory*, *Geophysical Monograph Series* (Vol. 138, pp. 83–105). Washington, DC: American Geophysical Union.

Hyndman, R. D. (2013). Downdip landward limit of Cascadia great earthquake rupture. *Journal of Geophysical Research*, *118*, 5530–5549. https://doi.org/10.1002/jgrb.50390

Hyndman, R. D., McCrory, P. A., Wech, A., Kao, H., & Ague, J. (2015). Cascadia subducting plate fluids channelled to fore-arc mantle corner: ETS and silica deposition. *Journal of Geophysical Research*, *120*, 4344–4358. https://doi.org/10.1002/2015JB011920.2015

Ide, S. (2010). Striations, duration, migration and tidal response in deep tremor. *Nature*, *466*, 356–359. https://doi.org/10.1038/nature09251

Ide, S. (2012). Variety and spatial heterogeneity of tectonic tremor worldwide. *Journal of Geophysical Research*, *117*, B03302. https://doi.org/10.1029/2011JB008840

Idehara, K., Yabe, S., & Ide, S. (2014). Regional and global variations in the temporal clustering of tectonic tremor activity. *Earth and Planetary Science Letters*, *66*, 66. https://doi.org/10.1186/1880-5981-66-66

Ji, Y., & Yoshioka, S. (2015). Effects of slab geometry and obliquity on the interplate thermal regime associated with the subduction of three-dimensionally curved oceanic plates. *Geoscience Frontiers*, *6*, 61–78. https://doi.org/10.1016/j.gsf.2014.04.011

Ji, Y., & Yoshioka, S. (2017). Slab dehydration and earthquake distribution beneath southwestern and central Japan based on three-dimensional thermal modeling. *Geophysical Research Letters*, *44*, 2679–2686. https://doi.org/10.1002/2016GL072295

Ji, Y., Yoshioka, S., & Matsumoto, T. (2016). Three-dimensional numerical modeling of temperature and mantle flow fields associated with subduction of the Philippine Sea plate, southwest Japan. *Journal of Geophysical Research: Solid Earth*, *121*, 4458–4482. https://doi.org/10.1002/2016JB012912

Ji, Y., Yoshioka, S., Manea, V. C., Manea, M., & Matsumoto, T. (2017). Three-dimensional numerical modeling of thermal regime and slab dehydration beneath Kanto and Tohoku, Japan. *Journal of Geophysical Research: Solid Earth*, *122*, 332–353. https://doi.org/10.1002/2016JB013230

Le Roux, V., Gaetani, G. A., Slaugenwhite, J., Miller, K. (2013). Fluids escape in subduction zones: New constraints from 3-D microtomography data, American Geophysical Union, Fall Meet. 2013, Abstract MR33A-2315.

Liu, Y. (2013). Numerical simulations on megathrust rupture stabilized under strong dilatancy strengthening in slow slip region. *Geophysical Research Letters*, *40*, 1311–1316. https://doi.org/10.1002/grl.50298

Liu, Y., & Rice, J. R. (2009). Slow slip predictions based on granite and gabbro friction data compared to GPS measurements in northern Cascadia. *Journal of Geophysical Research*, *114*, B09407. https://doi.org/10.1029/2008JB006142

McCaffrey, R., King, R. W., Payne, S. J., & Lancaster, M. (2013). Active tectonics of northwestern U.S. inferred from GPS-derived surface velocities. *Journal of Geophysical Research*, *118*, 709–723. https://doi.org/10.1029/2012JB009473

McCrory, P. A., Blair, J. L., Waldhauser, F., & Oppenheimer, D. H. (2012). Juan de Fuca slab geometry and its relation to Wadati-Benioff zone seismicity. *Journal of Geophysical Research*, *117*, B09306. https://doi.org/10.1029/2012JB009407

McCrory, P. A., Hyndman, R. D., & Blair, J. L. (2014). Relationship between the Cascadia fore-arc mantle wedge, nonvolcanic tremor, and the downdip limit of seismogenic rupture. *Geochemistry, Geophysics, Geosystems*, *15*, 1071–1095. https://doi.org/10.1002/2013GC005144

Miller, M. M., Melbourne, T. I., Johnson, D. J., & Summer, W. Q. (2002). Periodic slow earthquakes from the Cascadia subduction zone. *Science*, *295*(5564), 2423. https://doi.org/10.1126/science.1071193

Muller, R. D., Sdrolias, M., Gaina, C., & Roest, W. R. (2008). Age, spreading rates, and spreading asymmetry of the world's ocean crust. *Geochemistry, Geophysics, Geosystems*, *9*, Q04006. https://doi.org/10.1029/2007GC001743

Nakajima, J., & Hasegawa, A. (2016). Tremor activity inhibited by well-drained conditions above a megathrust. *Nature Communications*, *7*, 13863. https://doi.org/10.1038/ncomms13863

Nelson, A. R. (1992). Discordant ^{14}C ages from buried tidal-marsh soils in the Cascadia subduction zone, southern Oregon coast. *Quaternary Research*, *38*(1), 74–90. https://doi.org/10.1016/0033-5894(92)90031-D

Nelson, A. R., Kelsey, H. M., & Witter, R. C. (2006). Great earthquakes of variable magnitude at the Cascadia subduction zone. *Quaternary Research*, *65*, 354–365. https://doi.org/10.1016/j.yqres.2006.02.009

Omori, S., Kita, S., Maruyama, S., & Santosh, M. (2009). Pressure–temperature conditions of ongoing regional metamorphism beneath the Japanese Islands. *Gondwana Research*, *16*, 458–469. https://doi.org/10.1016/j.gr.2009.07.003

Peacock, S. M. (2009). Thermal and metamorphic environment of subduction zone episodic tremor and slip. *Journal of Geophysical Research*, *114*. B00A07. https://doi.org/10.1029/2008JB005978

Peacock, S. M., & Wang, K. (1999). Seismic consequences of warm versus cool subduction metamorphism: Examples from southwest and northeast Japan. *Science*, *286*(5441), 937–939. https://doi.org/10.1126/science.286.5441.937

Peacock, S. M., Christensen, N. I., Bostock, M. G., & Audet, P. (2011). High pore pressures and porosity at 35 km depth in the Cascadia subduction zone. *Geology*, *39*(5), 471. https://doi.org/10.1130/G31649.1

Plümper, O., John, T., Podladchikov, Y. Y., Vrijmoed, J. C., & Scambelluri, M. (2017). Fluid escape from subduction zones controlled by channel-forming reactive porosity. *Nature Geoscience*, *10*, 150–156. https://doi.org/10.1038/ngeo2865

Pollack, H. N., Hurter, S. J., & Johnson, J. R. (1993). Heat flow from the earth's interior: Analysis of the global data set. *Reviews of Geophysics*, *31*(3), 267–280. https://doi.org/10.1029/93RG01249

Rogers, G., & Dragert, H. (2003). Episodic tremor and slip on the Cascadia subduction zone: The chatter of silent slip. *Science*, *300*, 1942–1943. https://doi.org/10.1126/science.1084783

Satake, K., Shimazaki, K., Tsuji, Y., & Ueda, K. (1996). Time and size of a giant earthquake in Cascadia inferred from Japanese tsunami records of January 1700. *Nature*, *379*, 246–249. https://doi.org/10.1038/379246a0

Schmidt, D. A., & Gao, H. (2010). Source parameters and time-dependent slip distributions of slow slip events on the Cascadia subduction zone from 1998 to 2008. *Journal of Geophysical Research*, *115*, B00A18. https://doi.org/10.1029/2008JB006045

Siebert, L., Simkin, T., & Kimberly, P. (2010). *Volcanoes of the World* (3rd ed., pp. 568). Berkeley: Univ. of California Press.

Smith, W. H. F., & Sandwell, D. T. (1997). Global seafloor topography from satellite altimetry and ship depth soundings. *Science*, *277*, 1957–1962. https://doi.org/10.1126/science.277.5334.1956

Tackley, P. J., & Xie, S. (2003). Stag3D: A code for modeling thermo-chemical multiphase convection in Earth's mantle. In K. J. Bathe (Ed.), *Computational Fluid and Solid Mechanics 2003* (pp. 1524–1527). Amsterdam, Netherlands: Elsevier.

Tréhu, A. M., Blakely, R. J., & Williams, M. C. (2012). Subducted seamounts and recent earthquakes beneath the central Cascadia forearc. *Geology*, *40*(2), 103–106. https://doi.org/10.1130/G32460.1

Tsuji, Y., Ueda, K., & Satake, K. (1998). Japanese tsunami records from the January 1700 earthquake in the Cascadia subduction zone. *Journal of the Seismological Society of Japan*, *51*, 1–17. http://doi.org/10.4294/zisin1948.51.1_1

Wada, I., & Wang, K. (2009). Common depth of slab-mantle decoupling: Reconciling diversity and uniformity of subduction zones. *Geochemistry, Geophysics, Geosystems*, *10*, Q10009. https://doi.org/10.1029/2009GC002570

Wang, K., & Tréhu, A. M. (2016). Some outstanding issues in the study of great megathrust earthquakes—The Cascadia example. *Journal of Geodynamics*, *98*, 1–18.

Wang, P. L., Engelhart, S. E., Wang, K., Hawkes, A. D., Horton, B. P., Nelson, A. R., & Witter, R. C. (2013). Heterogeneous rupture in the great Cascadia earthquake of 1700 inferred from coastal subsidence estimates. *Journal of Geophysical Research*, *118*, 1–14. https://doi.org/10.1002/jgrb.50101

Wilson, C. R., Spiegelman, M., van Keken, P. E., & Hacker, B. R. (2014). Fluid flow in subduction zones: The role of solid rheology and compaction pressure, *Earth and Planetary Science Letters*, *401*, 261–274. https://doi.org/10.1016/j.epsl.2014.05.052

Yamaguchi, D. F., Atwater, B. F., Bunker, D. E., Benson, B. E., & Reid, M. S. (1997). Tree-ring dating the 1700 Cascadia earthquake. *Nature*, *389*, 922–923. https://doi.org/10.1038/40048